

## Atomic and electronic surface structures of dopants in oxides: STM and XPS of Nb- and La-doped SrTiO<sub>3</sub>(001)

Matthew S. J. Marshall,<sup>1,\*</sup> David T. Newell,<sup>1</sup> David J. Payne,<sup>2</sup> Russell G. Egdel,<sup>2</sup> and Martin R. Castell<sup>1,†</sup>

<sup>1</sup>*Department of Materials, University of Oxford, Parks Road, Oxford OX1 3PH, United Kingdom*

<sup>2</sup>*Department of Chemistry, University of Oxford, South Parks Road, Oxford OX1 3QR, United Kingdom*

(Received 9 September 2010; published 20 January 2011)

High resolution X-ray photoelectron spectroscopy (XPS) was performed on the (001) surfaces of Nb-doped and La-doped single crystals of SrTiO<sub>3</sub>. For the Nb-doped samples the XPS results demonstrate that the fraction of Ti<sup>3+</sup> ions increases with increasing Nb dopant concentration. The Nb dopants are shown to be in a 5+ ionization state. Atomic resolution scanning tunneling microscopy (STM) images of the 0.7 at.% Nb-doped SrTiO<sub>3</sub>(001) surface show that Nb-dopant atoms can be imaged on the surface as bright four-point square clusters. No evidence of Nb segregation to the (001) surface was found under ultrahigh vacuum (UHV) annealing. However, UHV annealing of the 0.7 at.% La-doped SrTiO<sub>3</sub>(001) samples at 1400 °C for 1 h resulted in La surface segregation as determined by Auger electron spectroscopy. STM on these samples shows that the segregated La results in La-rich linear surface structures.

DOI: [10.1103/PhysRevB.83.035410](https://doi.org/10.1103/PhysRevB.83.035410)

PACS number(s): 68.35.Dv, 68.35.Fx, 68.37.Ef

### I. INTRODUCTION

Interest in the doped perovskite SrTiO<sub>3</sub> has been stimulated by its photocatalytic properties,<sup>1</sup> use as an anode in solid oxide fuel cells<sup>2–4</sup> and in oxygen sensors,<sup>5</sup> and because of studies showing dopant-dependent blue photoluminescence.<sup>6</sup> Recent work has also demonstrated that SrTiO<sub>3</sub> has the potential to be a key component material in oxide-based electronic devices.<sup>7–12</sup> It is also a suitable substrate for the growth of thin films<sup>13</sup> and epitaxial islands.<sup>14,15</sup> Some exciting discoveries of the electrical transport properties of the SrTiO<sub>3</sub>-LaAlO<sub>3</sub> interface<sup>13,16–18</sup> have stimulated discussion as to whether this enhanced conductivity may be due to La diffusion into the SrTiO<sub>3</sub> near the interface.<sup>19–21</sup>

Undoped SrTiO<sub>3</sub> is an insulator with a 3.2 eV band gap. SrTiO<sub>3</sub> can be rendered conductive by doping, or by thermal reduction (doping with oxygen vacancies), facilitating experimental investigations that are not possible on insulating samples. The inclusion of either Nb or La dopants in SrTiO<sub>3</sub> results in *n*-type behavior. It is believed that this occurs by the substitution of Nb<sup>5+</sup> on a Ti<sup>4+</sup> site of the single crystal, or the substitution of La<sup>3+</sup> on a Sr<sup>2+</sup> site.<sup>22,23</sup>

Eight different reconstructions have been reported on the SrTiO<sub>3</sub>(001) surface following UHV annealing.<sup>24–27</sup> The prevailing model for many of these terminations is a double layer TiO<sub>2</sub> structure,<sup>28,29</sup> proposed by Erdman *et al.*<sup>24</sup> for the (2 × 1) reconstruction. Additionally, Ar<sup>+</sup> bombardment of the SrTiO<sub>3</sub>(001) surface followed by subsequent UHV annealing results in the formation of ordered Ti-rich nanostructures.<sup>30,31</sup> Extended UHV annealing gives rise to larger Ti-rich surface structures, including TiO islands<sup>32,33</sup> and single crystals of anatase TiO<sub>2</sub>.<sup>14,15</sup> Although the SrTiO<sub>3</sub>(001) surface structure has been thoroughly characterized, there are only a few studies on the effects that the dopants have on the electronic and atomic surface structure.<sup>44</sup> Adachi *et al.* used X-ray photoemission spectroscopy (XPS) to study UHV fractured, Ar<sup>+</sup> bombarded SrTiO<sub>3</sub>, as well as 1 at.% Nb-doped and 3 at.% La-doped SrTiO<sub>3</sub>(001).<sup>45</sup> Their work confirmed that UHV fractured samples contain Ti in the 4+ oxidation state, while Ar<sup>+</sup> bombarded samples showed a significant

Ti<sup>3+</sup> peak. XPS of reduced SrTiO<sub>3</sub> has also revealed that oxygen vacancy creation is accompanied by increases in the amount of Ti<sup>3+</sup>.<sup>46</sup> The work by Gunhold *et al.* on La-doped SrTiO<sub>3</sub> showed that annealing samples at high temperatures in reducing conditions for 150 h resulted in the segregation of La to the surface region,<sup>47</sup> where it became incorporated in large Ti<sub>2</sub>O<sub>3</sub> islands. Annealing 0.1 at.% La-doped SrTiO<sub>3</sub>(001) at 1000–1300 °C for 2 h did not show significant surface enrichment of La. In contrast, UHV annealing of 5 at.% La-doped SrTiO<sub>3</sub>(001) between 1000–1300 °C resulted in the formation of 20 nm diameter islands potentially consisting of LaTiO<sub>3</sub>.<sup>48</sup>

In contrast to SrTiO<sub>3</sub>, the effects of Nb doping in rutile TiO<sub>2</sub> have been studied extensively, motivated by reports that Nb doping enhances both the catalytic and photocatalytic activity of TiO<sub>2</sub>.<sup>34</sup> As in the case of SrTiO<sub>3</sub>, Nb atoms substitute for the Ti cations in the crystal. Unlike SrTiO<sub>3</sub>, NbO<sub>2</sub> forms a complete range of solid solutions with TiO<sub>2</sub>.<sup>35</sup> Moreover, Nb atoms are reported to add shallow donor states to the 3.06 eV band gap of rutile, 0.02–0.03 eV below the conduction band minimum.<sup>36</sup> Photoemission studies on rutile TiO<sub>2</sub> (110) performed by Morris *et al.*<sup>37</sup> demonstrate a well-defined Nb photoemission peak, which increases in intensity with rising doping levels. The authors show that Nb is incorporated within the rutile lattice, predominantly as Nb<sup>5+</sup>, and that the state introduced into the band gap is associated with the corresponding Ti<sup>3+</sup> ions. These results are correlated with STM images from the Nb-doped TiO<sub>2</sub>(110) surface. The STM images show the (1 × 1) reconstruction of the surface and a number of distinct clusters within this structure, each consisting of four bright spots. These clusters are interpreted as the visualization of charge transfer to four neighboring Ti surface atoms, which surround a Nb<sup>5+</sup> dopant atom. Using STM to study dopants has also been carried out on many other systems, including imaging of Li dopants on the NiO(001) surface,<sup>38</sup> Te and Si dopants in GaAs,<sup>39,40</sup> B dopants on a monohydride terminated Si surface [Si(100)-(2 × 1) : H],<sup>41</sup> and of Ni and Zn dopants in Bi<sub>2</sub>Sr<sub>2</sub>CaCu<sub>2</sub>O<sub>8+δ</sub> superconductors.<sup>42,43</sup>

In this paper, we use XPS to determine the dopant concentration in the surface region and to study the effects of doping on the oxidation state of Ti in SrTiO<sub>3</sub>(001). Furthermore, we show STM images of the Nb-doped SrTiO<sub>3</sub>(001) surface, in which the electronic structure of the dopant atom can be observed as a bright four-point cluster similar to those shown by Morris *et al.* on the Nb-doped TiO<sub>2</sub>(110) surface.<sup>37</sup> Lastly, we show that La-rich nanolines form on the SrTiO<sub>3</sub>(001) surface as a result of a surface segregation of the La dopant atoms after a 1 h UHV anneal at 1400 °C.

## II. EXPERIMENTAL

Single crystal epi-polished SrTiO<sub>3</sub>(001) samples were provided by PI-KEM Ltd., UK. These crystals were supplied with four different compositions: undoped SrTiO<sub>3</sub>, 0.5 wt.% Nb doped, 5.0 wt.% Nb doped, and 1.0 wt.% La doped. The crystals were outsourced from different crystal growers but differed only in their doping level. Although the crystals were ordered by their wt.% doping, it is more meaningful to evaluate their doping level as an at.% doping level of the ion that the dopant substitutes for, i.e., for 3 at.% of Nb dopant the stoichiometry of the crystal is SrTi<sub>0.97</sub>Nb<sub>0.03</sub>O<sub>3</sub>, for 3 at.% of La dopant the stoichiometry of the crystal is Sr<sub>0.97</sub>La<sub>0.03</sub>TiO<sub>3</sub>. Hence the nominal chemical compositions of the samples listed earlier are: undoped SrTiO<sub>3</sub>, 1 at.% Nb-doped SrTiO<sub>3</sub>, 10 at.% Nb-doped SrTiO<sub>3</sub>, and 1.3 at.% La-doped SrTiO<sub>3</sub>. Doping with Nb or La at these levels renders the samples sufficiently electrically conducting to allow STM and XPS to be performed on them.

The samples were introduced into the ultrahigh vacuum (UHV) preparation chamber of a JEOL JSTM4500S scanning tunneling microscope (STM) at a base pressure of 10<sup>-8</sup> Pa. A JEOL TM Z9043T UHV scanning electron microscope (SEM) and Auger electron spectrometer (AES) are in a UHV chamber attached to the JSTM4500S. The SEM was operated at an accelerating voltage of 12 kV. The SEM electron beam generates Auger electrons from the sample that are analyzed using a SPECS PHOIBOS 100 hemispherical analyzer. The signal-to-noise ratio of this system is sufficiently high so that Auger spectra can be recorded in terms of the primary signal without the need for differentiation or the use of a lock-in amplifier.

High-resolution X-ray photoemission spectra were obtained using an XPS spectrometer (Scienta ESCA 300) operated at the National Centre for Electron Spectroscopy and Surface Analysis (NCESS) at the Daresbury Laboratory, UK. The XPS system uses a rotating anode Al K $\alpha$  X-ray source, a seven-crystal X-ray monochromator, and a spherical sector electron energy analyzer with a mean radius of 300 mm and a channel plate electron detection system. This results in an effective instrument resolution of 350 meV. The ESCA 300 has facilities for electron-beam heating, which were used to prepare as-received samples for analysis by heating in UHV. Peak fitting was done using the XPSPEAK program, which determined the FWHM, peak location, and an optimal mix of Lorentzian versus Gaussian character that best fit the data within the constraints of the system.

## III. RESULTS

Figure 1 shows core level XPS spectra obtained from Nb-doped and La-doped SrTiO<sub>3</sub>. All XPS spectra were obtained following annealing as-received samples in UHV at 650 °C for 10–30 min. Comparing Ti peak heights to Nb peak heights indicates that the concentration of Nb was less than the manufacturer's specified doping levels.<sup>49,50</sup> The composition parameters of the doped SrTiO<sub>3</sub> samples were found to be 0.7 at.% instead of 1.0 at.% Nb doped, 6.0 at.% instead of 10.0 at.% Nb doped. Comparing Sr peaks with those of La resulted in a revision to 0.7 at.% La doped instead of 1.3 at.% La doped. From this point on, all samples will be referred to by the experimentally determined doping levels as those values are thought to be more reliable. Figure 1(a) shows a broad scan XPS spectrum of the 0.7 at.% La-doped sample with all the binding energy peaks indicated. A small carbon contamination peak is also visible at approximately 286 eV. Our experience with XPS and AES on SrTiO<sub>3</sub>(001) samples is that carbon contamination can only be completely removed by annealing in UHV at temperatures around 800 °C or above. However, these anneal temperatures give rise to oxygen loss from the surface region and hence result in reduced crystals. We specifically wanted to avoid this process, as sub-stoichiometric crystals contain Ti<sup>3+</sup> ions which interfere with our interpretation of the effects of the dopants.

Figure 1(b) shows the binding energy peaks of the Ti 2p states of the 0.7 at.% Nb-doped sample. The Nb 3d peaks from the same sample are shown in Fig. 1(e). The Nb 3d<sub>5/2</sub> core level binding energies in Figs. 1(e) and 1(f) were measured at 208.0 ± 0.1 eV and 207.8 ± 0.1 eV, where the listed error refers to the accuracy of measuring energies of fitted peak maxima. These values are the same as the Nb 3d<sub>5/2</sub> binding energies in Nb<sub>2</sub>O<sub>5</sub> crystals. This indicates that Nb dopes into SrTiO<sub>3</sub> as Nb<sup>5+</sup> with the additional valence charge of the Nb dopants distributed amongst adjacent Ti atoms as can be seen in the XPS spectra from the highly doped 6 at.%Nb-doped sample shown in Figs. 1(c) and 1(f). In Fig. 1(c) the Ti 2p peak at a binding energy of 457.5 ± 0.1 eV is associated with the creation of Ti<sup>3+</sup> ions due to the Nb dopants. A smaller but well-defined Ti<sup>3+</sup> peak is clearly visible in the expanded spectrum for the lower dopant level [Fig. 1(b)], and is also identified during the peak fitting.

Experiments on the La-doped sample reveal the La core level 3d peaks depicted in Fig. 1(g). The peaks are situated at 835.4 ± 0.1 eV, 839.4 ± 0.1 eV, 852.2 ± 0.1 eV, and 856.3 ± 0.1 eV which correspond to La in the 3+ state. As for the case of Nb, the excess La valence electron is located on the neighboring Ti ions, giving rise to a Ti<sup>3+</sup> state. The Ti 2p core level peaks corresponding to the La-doped sample are depicted in Fig. 1(d) and are located at 459.3 ± 0.1 eV for Ti<sup>4+</sup>, and 457.3 ± 0.1 eV for Ti<sup>3+</sup>, the latter of which is readily visible in the magnified spectrum.

SrTiO<sub>3</sub>(001) crystal surfaces with a ( $\sqrt{5} \times \sqrt{5}$ )-R26.6° reconstruction can be generated by UHV annealing at temperatures of between 1350–1450 °C. This surface is thought to be the result of phase separation in the surface region due to high levels of oxygen depletion,<sup>33</sup> and the surface has been modelled as an ordered overlayer of Sr adatoms.<sup>27</sup> Once the reconstruction has been created it can be reannealed

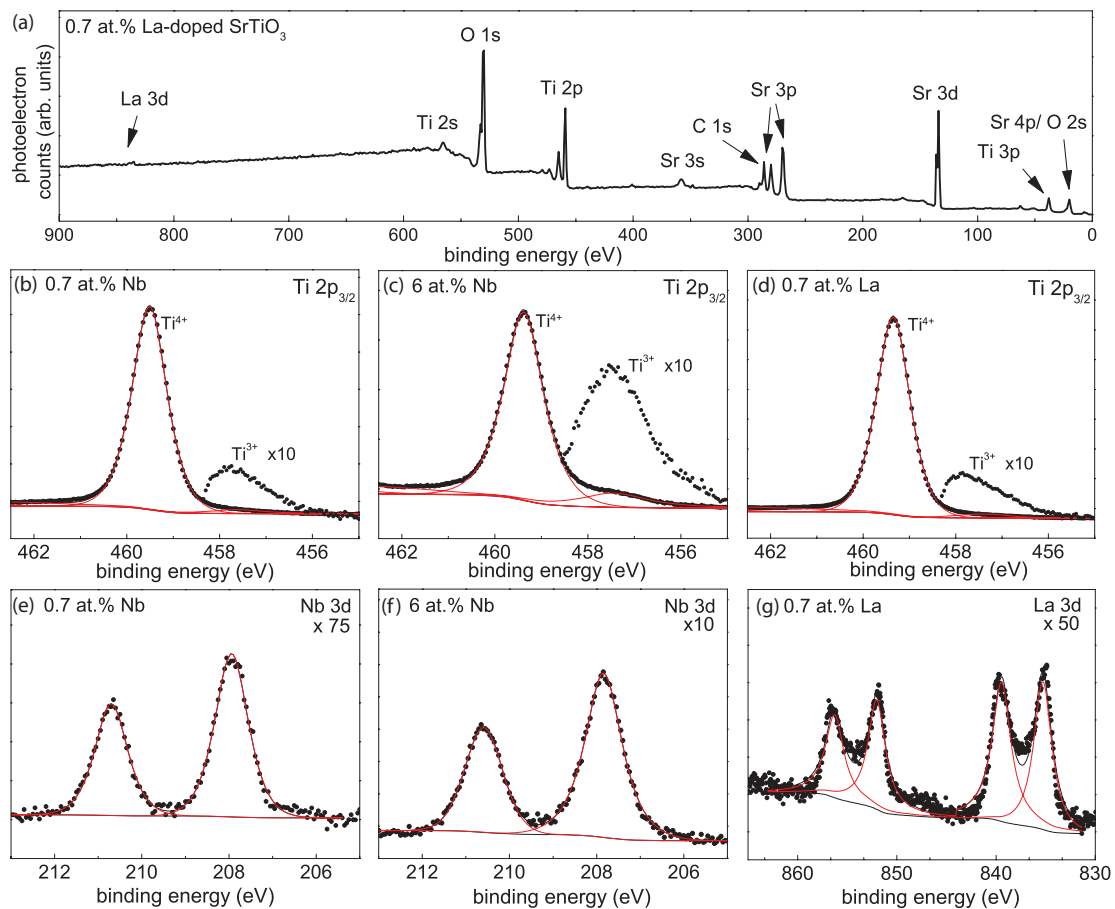


FIG. 1. (Color online) An Al  $K\alpha$  core level XPS survey is shown for a 0.7 at.% La-doped  $\text{SrTiO}_3$  sample in (a) with all the major peaks indicated. The Ti  $2p$  peaks for 0.7 at.% Nb-doped, 6.0 at.% Nb-doped, and 0.7 at.% La-doped  $\text{SrTiO}_3$  are shown in (b)–(d). The  $\text{Ti}^{3+}$  structure is shown in (b)–(d) expanded by a factor of 10 after subtraction of the  $\text{Ti}^{4+}$  peak. The Nb  $3d$  peaks are shown in (e) and (f), and the La  $3d$  peak is shown in (g). For each spectrum the doping level is indicated in the top left-hand corner of the box, and the electronic state that the peaks correspond to is indicated in the top right. The thin lines (colored red online) correspond to the fitted peaks over a Shirley background.

in UHV at lower temperatures which allows the Sr adatoms to reoxidize and form an SrO overlayer. In our experiments we have annealed a  $(\sqrt{5} \times \sqrt{5})\text{-R}26.6^\circ$  reconstructed sample of 0.7 at.% Nb-doped  $\text{SrTiO}_3$  below  $1100^\circ\text{C}$  which results in the SrO-terminated  $(1 \times 1)$  reconstructed surface shown in Fig. 2. The SrO  $(1 \times 1)$  surfaces are decorated with bright four-point clusters, believed to occur as a result of subsurface Nb dopant atoms. The density of bright four-point clusters on the surface of the  $(1 \times 1)$  reconstruction was  $(0.051 \pm 0.013)/\text{nm}^2$  which is within experimental error of the value indicated by the XPS data. The spots constituting the clusters in Fig. 2(b) and 2(c) are aligned along the  $[100]$  and  $[010]$  axes of the crystal. The four-point clusters are only seen on parts of the surface that have an SrO  $(1 \times 1)$  overlayer. Measurement of the separation of the spots in the clusters shows that it corresponds to that of a single  $\text{SrTiO}_3$  unit cell. In addition to the  $(1 \times 1)$  SrO termination, samples were often seen with a second type of structure on the surface. In Fig. 2(b) this second region has the resemblance of a disordered leopard spotted pattern, and no four-point clusters can be seen here. It should also be noted that imaging the  $(1 \times 1)$  overlayer was relatively difficult.

Even the best images have a streaky appearance along the fast scan direction which is indicative of a surface where the topmost monolayer is electrically insulating.

STM was also used to investigate surface segregation in the La doped samples, as shown in Fig. 3(a) where five bright nanoline features are randomly distributed across the disordered surface of 0.7 at.% La-doped  $\text{SrTiO}_3$ . This surface was prepared by annealing a  $c(4 \times 4)$  reconstructed surface for 1 h at  $1400^\circ\text{C}$ . A nanoline is shown at a higher magnification in Fig. 3(b) and consists of four distinct rows of bright spots. The majority of the lines observed on the sample were orientated in the same direction as those seen in Fig. 3(a). Annealing at lower temperatures did not result in the nanoline features. For example, a 0.7 at.% La-doped  $\text{SrTiO}_3$  sample annealed in UHV for 1 h at  $1300^\circ\text{C}$  resulted in a flat surface with no discernible surface order.

Figure 4(a) shows broad range AES spectra for  $\text{SrTiO}_3(001)$  samples that have been subjected to different preparation methods. The peaks at 380 and 413 eV arise from Ti (LMM), the peaks at 492 and 511 eV from O (KLL), and the peaks at 1644 and 1711 eV from Sr (LMM). The UHV-cleaved

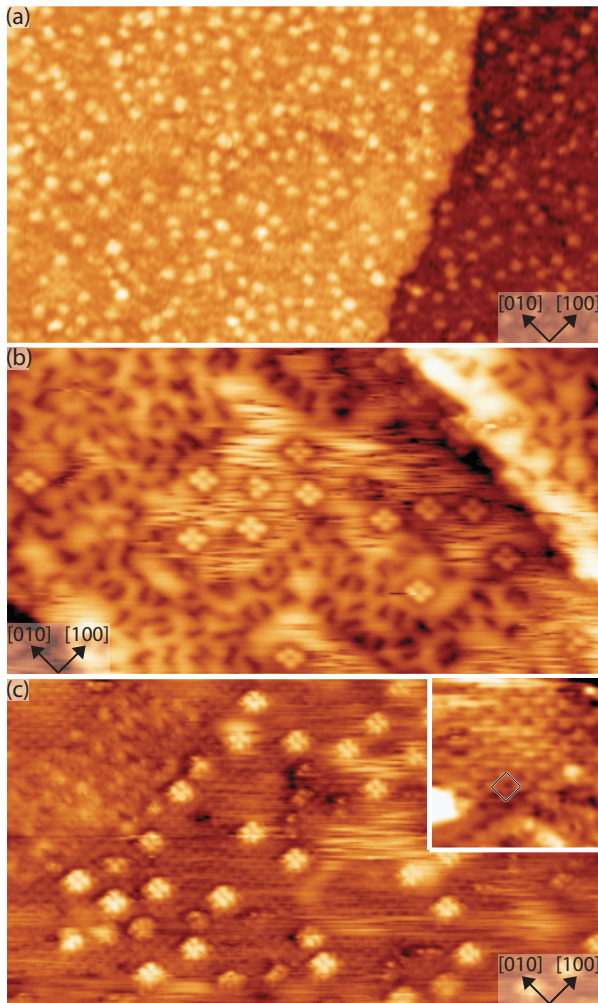


FIG. 2. (Color online) STM images of 0.7 at.% Nb-doped  $\text{SrTiO}_3$  covered with an SrO overlayer. (a) STM image showing two flat terraces separated by a step edge of  $\text{SrTiO}_3(001)$  unit cell height (approximately 0.4 nm). Bright spots, thought to be due to the Nb dopants, are uniformly distributed across both terraces ( $69.5 \times 39.4 \text{ nm}^2$ ,  $V_s = 0.8 \text{ V}$ ,  $I_t = 0.1 \text{ nA}$ ). (b) An STM image in which the bright spots are visible as four-point clusters ( $23.1 \times 13 \text{ nm}^2$ ,  $V_s = 1.0 \text{ V}$ ,  $I_t = 0.3 \text{ nA}$ ). (c) STM image showing bright four-point clusters, where the  $(1 \times 1)$  periodicity of the surrounding surface can be resolved ( $23.6 \times 13.5 \text{ nm}^2$ ,  $V_s = 1.0 \text{ V}$ ,  $I_t = 1.0 \text{ nA}$ ). Inset in (c) is an enlarged image of the top left corner of (c), in which the square unit cell of an ordered  $(1 \times 1)$  domain is shown ( $4.3 \times 4.3 \text{ nm}^2$ ,  $V_s = 1.0 \text{ V}$ ,  $I_t = 1.0 \text{ nA}$ ).

spectrum (dotted line) is from a 0.7 at.% Nb-doped crystal and serves as a baseline for comparison purposes. The thin line is a spectrum of a 0.7 at.% La-doped sample that was annealed in UHV for 1 h at  $1300^\circ\text{C}$  and shows no surface features in the STM images. However, by annealing the La-doped sample in UHV for 1 h at  $1400^\circ\text{C}$  a distinct Auger peak at 625 eV is apparent which corresponds to the La MNN transition. The La Auger peak is only visible for samples that also show the type of nanolines seen in the STM images of Fig. 3. In Fig. 4(b), a higher magnification of the spectra from 525–725 eV show in more detail the La (MNN) peak at 625 eV exhibited by the sample with nanolines. The emergence of the La Auger

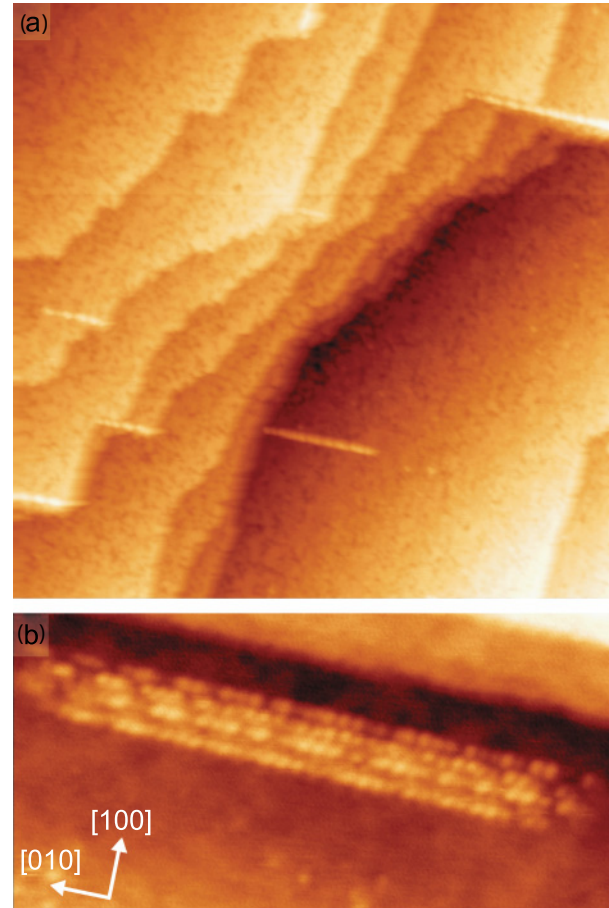


FIG. 3. (Color online) (a) STM image taken from a 0.7 at.% La-doped  $\text{SrTiO}_3(001)$  sample showing a cluster of step edges and bright white nanoline features oriented along the  $[010]$  direction ( $170 \times 170 \text{ nm}^2$ ,  $V_s = 1.0 \text{ V}$ ,  $I_t = 0.3 \text{ nA}$ ). (b) A high resolution STM image showing the detail of a La nanoline ( $70 \times 35 \text{ nm}^2$ ,  $V_s = 0.4 \text{ V}$ ,  $I_t = 0.3 \text{ nA}$ ).

peak in conjunction with the appearance of the nanolines on the surface indicates that the bright nanolines of Fig. 3 are composed of segregated La dopants. Similar experiments for Nb-doped samples showed no evidence of Nb segregation.

#### IV. DISCUSSION

In this paper we have presented results that elucidate the behavior of Nb and La  $n$ -type dopants in  $\text{SrTiO}_3$ . XPS, STM, and AES were used to study the dopant ionization states, image the dopant distributions, and demonstrate surface segregation phenomena. In particular, XPS shows that Nb dopes in the 5+ state, La in the 3+ state, and charge compensation for both dopants is achieved via  $\text{Ti}^{3+}$  states. While these results are in line with expectations, it is nevertheless reassuring to demonstrate consistency with the standard concept that  $\text{Nb}^{5+}$  ions are located substitutionally on Ti sites and  $\text{La}^{3+}$  ions are located substitutionally on Sr sites, and that valence charge transfer to surrounding Ti ions gives rise to  $\text{Ti}^{3+}$  states. XPS shows a direct correlation between the dopant concentrations and the  $\text{Ti}^{3+}$  peak intensity. The dopant levels were measured to be lower than specified by the crystal grower, and we

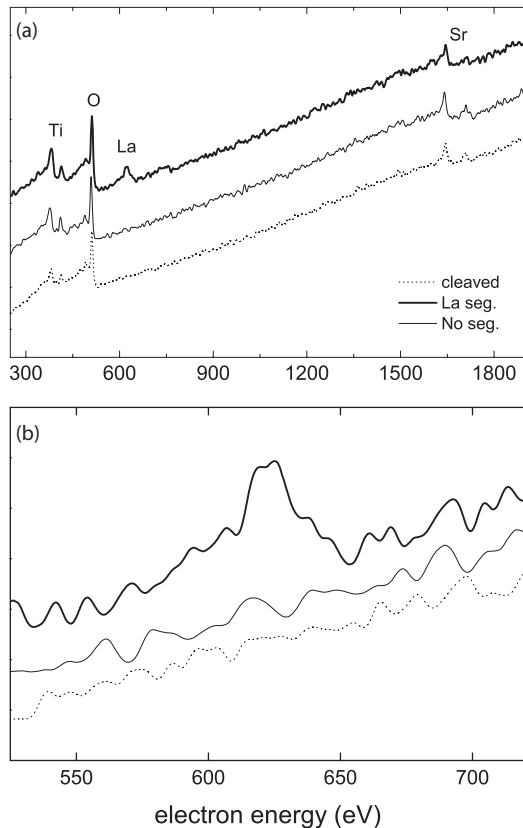


FIG. 4. Auger spectra of SrTiO<sub>3</sub>(001) obtained following differing surface preparation procedures. In (a) broad-range spectra are shown of UHV cleaved (spotted line), UHV annealed La-doped sample at 1300 °C (thin line), and UHV annealed La-doped sample at 1400 °C (thick line) decorated with the type of nanolines show in Fig. 3. The peaks are labeled relating to Ti (LMM) at 380 and 413 eV, O (KLL) at 492 and 511 eV, La (MNN) 625 eV, and Sr (LMM) at 1644 and 1711 eV. All spectra were normalized such that the value of each spectrum at 1100 eV in the featureless background region was set to the same value. Then, the spectra were offset from each other to facilitate viewing. A magnified region of the AES spectra around the La peak is shown in (b).

speculate that this is due to the difference between the level of dopant added to the melt during growth and the level of dopant that is eventually incorporated onto substitutional lattice sites in the crystal.

The appearance of Nb dopants as four-point clusters in the STM images is somewhat unusual, but consistent with other studies of Nb dopants in titanates.<sup>37</sup> Our interpretation of the clusters in the images is that the Nb dopants are located substitutionally on Ti lattice sites that are in a TiO<sub>2</sub> monolayer just below the top SrO (1×1) surface. The Nb dopants are equidistant from four surface Sr ions, and so affect them equally, and hence each Nb dopant is responsible for a four-point cluster. There is no evidence of charge transfer to the four Sr surface atoms, and indeed this would be very unexpected. What is more likely is that this is an electrostatic effect due to the local potential around the Nb dopant, or possibly some other more subtle electronic structure perturbation. A point of significance in the STM images is that the four-point clusters are only ever seen on a surface

that has a scratchy appearance which is an indication of an insulating top monolayer, consistent with SrO being the top monolayer. However the four-point clusters do not have a scratchy appearance. This leads us to conclude that the electronic states due to the Nb dopants that are being probed by the STM lie within the bandgap of the SrO surface monolayer. These Nb dopant states are not seen on the parts of the crystal surface that do not have an SrO termination and have a smaller bandgap, and the dopant states fall outside the bandgap and are hence a lot less easy to image. Much of the above is speculative, and detailed electronic structure calculations are required to properly address the question of the origin of the Nb induced four-point clusters.

By annealing the 0.7 at.% Nb and La-doped SrTiO<sub>3</sub> samples we have demonstrated the difference in segregation behavior of Nb and La. No evidence of Nb segregation is detected at UHV anneal temperatures up to 1500 °C. However, a 1400 °C anneal of the La-doped samples results in the formation of La-rich linear surface structures. These structures bear a resemblance to the Ca impurity induced nanolines described by Polli *et al.*,<sup>51</sup> but calcium segregation can be ruled out in our samples because Ca is readily detectable in Auger spectra at 291 eV, and a peak is entirely absent from Fig. 4. The linear appearance of the La nanostructures is most likely because they form at or stabilize <100> type step edges. At the high anneal temperatures the steps can migrate, resulting in freestanding linear La structures. It is also interesting that the La segregation gives rise to a disordered surface, and the ( $\sqrt{5} \times \sqrt{5}$ )-R26.6° reconstruction is not seen, although this reconstruction is routinely created on Nb-doped samples that have undergone the same processing procedure. Presumably the La segregation disrupts the formation of the ( $\sqrt{5} \times \sqrt{5}$ )-R26.6° reconstruction. The phenomenon of surface segregation can be driven by a broad host of mechanisms varying from lattice strain reduction around dopants to surface energy minimization. Given the numerous possibilities it would be unwise to speculate on why La segregates but Nb does not.

## V. CONCLUSION

In summary, our XPS studies of doped SrTiO<sub>3</sub> crystals have revealed that a Ti<sup>3+</sup> state arises due to charge compensation of the Nb<sup>5+</sup> and La<sup>3+</sup> dopants. We have also shown STM images of four-point clusters related to subsurface Nb dopants, and demonstrated that at high anneal temperatures La segregates to the (001) surface but Nb does not. These studies provide part of the basic underpinning understanding that is necessary for perovskite oxides to be fully exploited for their functional properties. For research areas such as oxide electronics to reach their potential a thorough understanding of dopant behavior in these materials is essential.

## ACKNOWLEDGMENTS

The authors would like to thank Chris Spencer (JEOL UK), Danny Law (NCESS) for technical support, and EPSRC and JEOL UK for funding. The NCESS facility at Daresbury Laboratory is supported by EPSRC grant no. EP/E025722/1. D.J.P. is supported by a Junior Research grant at Christchurch College, Oxford.

\*Present address: CRISP, Department of Applied Physics, Yale University, New Haven, CT.

†martin.castell@materials.ox.ac.uk

- <sup>1</sup>J. G. Mavroides, J. A. Kafalas, and D. F. Kolesar, *Appl. Phys. Lett.* **28**, 241 (1976).
- <sup>2</sup>J. C. Ruiz-Morales, J. Canales-Vázquez, C. Savaniu, D. Marrero-López, and W. Zhou, J. T. S. Irvine, *Nature (London)* **439**, 568 (2006).
- <sup>3</sup>O. A. Marina and N. L. Canfield, and J. W. Stevenson, *Solid State Ionics* **149**, 21 (2002).
- <sup>4</sup>J. Canales-Vázquez, S. W. Tao, and J. T. S. Irvine, *Solid State Ionics* **159**, 159 (2003).
- <sup>5</sup>W. Menesklo, H. J. Schreiner, K. H. Härdtl, and E. Ivers-Tiffée, *Sensors & Actuators: B Chemical* **59**, 184 (1999).
- <sup>6</sup>D. Kan, R. Kanda, Y. Kanemitsu, Y. Shimakawa, M. Takano, T. Terashima, and A. Ishizumi, *Appl. Phys. Lett.* **88**, 191916 (2006).
- <sup>7</sup>C. Cen, S. Theil, J. Mannhard, and J. Levy, *Science* **323**, 1026 (2009).
- <sup>8</sup>D. W. Reagor and V. Y. Butko, *Nat. Mater.* **4**, 593 (2005).
- <sup>9</sup>H. Ohta, S. W. Kim, Y. Mune, T. Mizoguchi, K. Nomura, S. Ohta, T. Nomura, Y. Nakanishi, Y. Ikuhara, M. Hirano, H. Hosono, and K. Koumoto, *Nat. Mater.* **6**, 129 (2007).
- <sup>10</sup>D. Kan, T. Terashima, R. Kanda, A. Masuno, K. Tanaka, S. Chu, H. Kan, A. Ishizumi, Y. Kanemitsu, Y. Shimakawa, and M. Takano, *Nat. Mater.* **4**, 816 (2005).
- <sup>11</sup>K. Szot, W. Speier, G. Bihlmayer, and R. Waser, *Nat. Mater.* **5**, 312 (2006).
- <sup>12</sup>K. Szot, R. Dittmann, W. Speier, and R. Waser, *Phys. Status Solidi (RRL)* **1**, R86 (2007).
- <sup>13</sup>A. Ohtomo and H. Y. Hwang, *Nature (London)* **427**, 423 (2004).
- <sup>14</sup>F. Silly and M. R. Castell, *Appl. Phys. Lett.* **85**, 3223 (2004).
- <sup>15</sup>M. S. J. Marshall and M. R. Castell, *Phys. Rev. Lett.* **102**, 146102 (2009).
- <sup>16</sup>N. Reyren, S. Thiel, A. D. Caviglia, L. Fitting Kourkoutis, G. Hammerl, C. Richter, C. W. Schneider, T. Kopp, A.-S. Rüetschi, D. Jaccard, M. Gabay, D. A. Muller, J.-M. Triscone, and J. Mannhart, *Science* **317**, 1196 (2007).
- <sup>17</sup>A. Brinkman, M. Huijben, M. van Zalk, J. Huijben, U. Zeitler, J. C. Maan, W. G. van der Wiel, G. Rijnders, D. H. A. Blank, and H. Hilgenkamp, *Nat. Mater.* **6**, 493 (2007).
- <sup>18</sup>J. W. Reiner, F. J. Walker, and C. H. Ahn, *Science* **323**, 1018 (2009).
- <sup>19</sup>P. R. Willmott, S. A. Pauli, R. Herger, C. M. Schlepütz, D. Martoccia, B. D. Patterson, B. Delley, R. Clarke, D. Kumah, C. Cionca, and Y. Yacoby, *Phys. Rev. Lett.* **99**, 155502 (2007).
- <sup>20</sup>Y. Segal, J. H. Ngai, J. W. Reiner, F. J. Walker, and C. H. Ahn, *Phys. Rev. B* **80**, 241107(R) (2009).
- <sup>21</sup>S. A. Chambers (private communication).
- <sup>22</sup>H. P. R. Frederikse and W. R. Hosler, *Phys. Rev.* **161**, 822 (1967).
- <sup>23</sup>N. G. Eror and U. Balachandran, *J. Solid State Chem.* **40**, 85 (1981).
- <sup>24</sup>N. Erdman, K. R. Poeppelmeier, M. Asta, O. Warschkow, D. E. Ellis, and L. D. Marks, *Nature (London)* **419**, 55 (2002).
- <sup>25</sup>F. Silly, D. T. Newell, and M. R. Castell, *Surf. Sci.* **600**, 219 (2006).
- <sup>26</sup>M. R. Castell, *Surf. Sci.* **505**, 1 (2002).
- <sup>27</sup>T. Kubo and H. Nozoye, *Phys. Rev. Lett.* **86**, 1801 (2001).
- <sup>28</sup>R. Herger, P. R. Willmott, O. Bunk, C. M. Schlepütz, B. D. Patterson, and B. Delley, *Phys. Rev. Lett.* **98**, 076102 (2007).
- <sup>29</sup>N. Erdman, O. Warschkow, M. Asta, K. R. Poeppelmeier, D. E. Ellis, and L. D. Marks, *J. Am. Chem. Soc.* **125**, 10050 (2003).
- <sup>30</sup>M. R. Castell, *Surf. Sci.* **516**, 33 (2002).
- <sup>31</sup>D. S. Deak, F. Silly, D. T. Newell, and M. R. Castell, *J. Phys. Chem. B* **110**, 9246 (2006).
- <sup>32</sup>S. B. Lee, F. Phillipp, W. Sigle, and M. Rühle, *Ultramicroscopy* **104**, 30 (2005).
- <sup>33</sup>D. T. Newell, A. Harrison, F. Silly, and M. R. Castell, *Phys. Rev. B* **75**, 205429 (2007).
- <sup>34</sup>H. Cui, K. Dwight, S. Soled, and A. J. Wold, *Solid State Chem.* **115**, 187 (1995).
- <sup>35</sup>K. Sakata, *J. Phys. Soc. Jpn.* **26**, 867 (1969).
- <sup>36</sup>T. Okamura and T. Okushi, *Jpn. J. Appl. Phys.* **32**, L454 (1993).
- <sup>37</sup>D. Morris, Y. Dou, J. Rebane, C. E. J. Mitchell, R. G. Egde, D. S. L. Law, A. Vittadini, and M. Casarin, *Phys. Rev. B* **61**, 13445 (2000).
- <sup>38</sup>M. R. Castell, P. L. Wincott, N. G. Condon, C. Muggelberg, G. Thornton, S. L. Dudarev, A. P. Sutton, and G. A. D. Briggs, *Phys. Rev. B* **55**, 7859 (1997).
- <sup>39</sup>J. Gebauer, E. R. Weber, N. D. Jäger, K. Urban, and P. Ebert, *Appl. Phys. Lett.* **82**, 2059 (2003).
- <sup>40</sup>C. Domke, P. Ebert, M. Heinrich, and K. Urban, *Phys. Rev. B* **54**, 10288 (1996).
- <sup>41</sup>L. Liu, J. Yu, and J. W. Lyding, *Appl. Phys. Lett.* **78**, 386 (2001).
- <sup>42</sup>E. W. Hudson, K. M. Lang, V. Madhavan, S. H. Pan, H. Eisaki, S. Uchida, and J. C. Davis, *Nature (London)* **411**, 920 (2001).
- <sup>43</sup>S. H. Pan, E. W. Hudson, K. M. Lang, H. Eisaki, S. Uchida, and J. C. Davis, *Nature (London)* **403**, 746 (2000).
- <sup>44</sup>T. Higuchi, T. Tsukamoto, N. Sata, M. Ishigame, Y. Tezuka, and S. Shin, *Phys. Rev. B* **57**, 6978 (1998).
- <sup>45</sup>Y. Adachi, S. Kohikia, K. Wagatsuma, and M. Oku, *J. Appl. Phys.* **84**, 2123 (1998).
- <sup>46</sup>H. L. Cai, X. S. Wub, and J. Gao, *Chem. Phys. Lett.* **467**, 313 (2009).
- <sup>47</sup>A. Gunhold, L. Beuermann, M. Frerichs, V. Kempter, K. Gömann, and G. Borchardt, W. Maus-Friedrichs, *Surf. Sci.* **523**, 80 (2003).
- <sup>48</sup>A. Gunhold, K. Gömann, L. Beuermann, V. Kempter, G. Borchardt, and W. Maus-Friedrichs, *Anal. Bioanal. Chem.* **375**, 924 (2003).
- <sup>49</sup>C. D. Wagner, L. E. Davis, M. V. Zeller, J. A. Taylor, R. H. Raymond, and L. H. Gale, *Surf. Interface Anal.* **3**, 211 (1981).
- <sup>50</sup>D. Briggs and M. P. Shea, *Practical Surface Analysis by Auger and X-ray Photoelectron Spectroscopy* (John Wiley & Sons, Chichester, 1983).
- <sup>51</sup>A. D. Polli, T. Wagner, and M. Rühle, *Surf. Sci.* **429**, 237 (1999).